ADVANCED MATERIALS
www.advmat.de

Target Reprogramming Lysosomes of CD8+ T Cells by a Mineralized Metal–Organic Framework for Cancer Immunotherapy

*Qin Zhao, Zijian Gong, Zhihao Li, Jinyang Wang, Jinglun Zhang, Zifan Zhao, Peng Zhang, Shihang Zheng, Richard J. Miron, Quan Yuan, and Yufeng Zhang**

T cell immunotherapy holds significant challenges in solid tumors, mainly due to the T cells' low activation and the decreased synthesis–release of therapeutic proteins, including perforin and granzyme B, which are present in lysosomes. In this study, a lysosome-targeting nanoparticle (LYS-NP) is developed by way of a mineralized metal–organic framework (MOF) coupled with a lysosome-targeting aptamer (CD63-aptamer) to enhance the antitumor effect of T cells. The MOF synthesized from Zn^{2+} and dimethylimidazole has good protein encapsulation and acid sensitivity, and is thus an ideal lysosomal delivery vector. Calcium carbonate ($CaCO_3$) is used to induce MOF mineralization, improve the composite material's stability in encapsulating therapeutic protein, and provide calcium ions with synergistic effects. Before mineralization, perforin and granzyme B—T cell-needed therapeutic proteins for tumors—are preloaded with the MOF. Moreover, T cells are pretreated with processed tumor-specific antigens to activate or produce memory before reprogramming the lysosomes, facilitating the T cell receptor (TCR) for release of the therapeutic proteins. Using T cells recombined by LYS-NPs, a significant enhancement of breast cancer control is confirmed.

1. Introduction

The relevance of T cells in cancer control is now beyond doubt. The immunotherapy that encourages the T cell to ruin tumor cells has established therapeutic efficacy in human malignancies. The typical procedure is to isolate T cells from the patient's peripheral blood, activate and enhance tumor specificity by biological or genetic engineering techniques, and then inject back to peripheral blood after expansion. This immunotherapy based on the adoptive transfer of engineered T cells is called adoptive T cell therapy, including chimeric antigen receptor (CAR)-T cells, tumor-infiltrating lymphocyte (TIL), and endogenous T cell (ETC) therapy.[1] Although adoptive T cell immunotherapy has been approved for B cell lymphoma treatment, it is less successful in solid tumors. This difficulty is partly due to the adoptive T cells are subjected to immunosuppression in the solid tumor. The suppressed T cells showing weak tumor targeting and low activation, resulting in a sharp reduction of potent toxins in the tumor area. These toxins, including perforin and granzyme B, are mainly secreted by cytotoxic T lymphocytes (CTLs, T cells expressing CD8) and partly natural killer cells (NK cells) after activation.[2] Once the activated $CD8^+$ T cells bind to the target cells (tumor cells), the former will release perforin and granzyme B into the attached cells' interstices. The interstices are called the immunological synapses.[3]

Dr. Q. Zhao, Z. Gong, J. Wang, J. Zhang, Z. Zhao, P. Zhang, S. Zheng, Prof. Y. Zhang
The State Key Laboratory Breeding Base of Basic Science of Stomatology (Hubei-MOST) & Key Laboratory of Oral Biomedicine Ministry of Education
School & Hospital of Stomatology
Wuhan University
Wuhan 430079, China
E-mail: zyf@whu.edu.cn

Dr. Q. Zhao, Z. Gong, J. Wang, J. Zhang, Z. Zhao, P. Zhang, S. Zheng, Prof. Y. Zhang
Medical Research Institute
School of Medicine
Wuhan University
Wuhan 430071, China

Dr. Z. Li, Prof. Q. Yuan
Key Laboratory of Analytical Chemistry for Biology and Medicine (Ministry of Education)
College of Chemistry and Molecular Sciences
Wuhan University
Wuhan 430072, China

Prof. R. J. Miron
Department of Periodontology
University of Bern
Bern 3010, Switzerland

The ORCID identification number(s) for the author(s) of this article can be found under https://doi.org/10.1002/adma.202100616.

DOI: 10.1002/adma.202100616

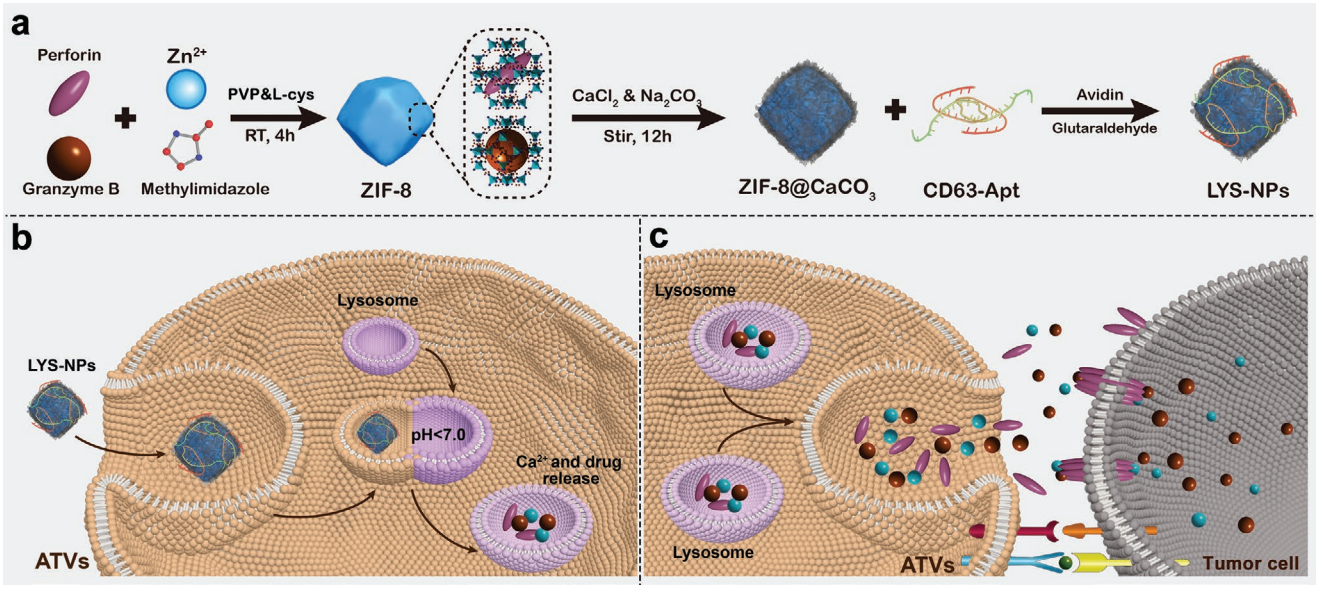

Scheme 1. Schematic diagram of the design and synthesis of LYS-NPs and their function. a) Schematic diagram of LYS-NPs synthetic processes. b) Schematic illustration of preparing ATVs with LYS-NPs. Once LYS-NPs are taken up by ATVs, they target $CD63^+$ lysosomes and degrade inside to release the contents stored in the lysosomes. c) Schematic of ATVs casting cytotoxic proteins and Ca^{2+} in reassembled lysosomes to kill target tumor cells.

Perforating the tumor cell membrane should induce tumor cell apoptosis and kill them. Therefore, perforin and granzyme B are the core weapons of the immune system against tumors.

The latest advances in nanotechnology and bioengineering technology provide a new and promising strategy for solid tumors' T cell immunotherapy.[4–8] Nanomaterials and bioengineering methods have been successfully applied for engineered $CD8^+$ T cells targeted to cancer sites or cancer cells.[9,10] These approaches focus on the specific activation of $CD8^+$ T cells in the tumor immune response and target cell binding capacity. For example, Tyrel et al. used a DNA nanocarrier to infuse $CD8^+$ T cells for DNA programming to enhance tumor cells' effect and specificity.[11] In addition to this type of method that uses nanotechnology to program functional gene fragments of CD8+ T cells directly, Stephan and his colleagues first adopted a "backpack" technology. They coupled the nanoparticles loaded with drugs to the surface of $CD8^+$ T cells to deliver drugs in the tumor area and enhance their immunotherapeutic effects.[12] Since then, the "backpack" technology of $CD8^+$ T cells has made some progress in a short time for tumor immunotherapy.[13–15] However, T cell immunotherapy based on nano-engineering for solid tumors still faces enormous challenges because of the tumor solidity and immunosuppression. It shows deficient T cells targeting the tumor area and the sharp decline in the synthesis and release of cytotoxic proteins — including perforin and granzyme B located in lysosomes. Herein, we propose an effective anti-solid-tumor strategy to enhance perforin and granzyme B's secretion by constructing a nano-engineered effector and memory $CD8^+$ T cells.

Metal–organic frameworks (MOFs) are a kind of porous materials assembled from metal/metal clusters and organic ligands.[16] Due to their unique properties, MOFs have been intensely studied and applied in many fields, including gas storage, catalysis, and chemical separation.[17] Recently, MOFs have made significant progress in the medical field, especially in drug delivery, mainly due to their high stability, high drug loading capacity, and pH sensitivity.[18,19] Among them, scientists found that ZIF-8 (made of Zn^{2+} ions connected by 2-methylimidazole (MIM) bridging units) can be synthesized by the co-precipitation method to encapsulate protein into the material directly.[20,21] Compared with merely adsorbing protein on the surface of materials, this method has higher entrapment efficiency and more vital protection for protein. Simultaneously, the material can be synthesized in a short time in the aqueous environment at room temperature, which effectively avoids the inactivation of protein.[22] Therefore, ZIF-8 is an ideal protein encapsulation and delivery carrier.

As proof of concept, we designed a lysosome-responsive nanoparticle (LYS-NP) loaded with anticancer proteins, which can target adoptive T cell lysosomes. We named this T cell that uses lysosomes to carry anticancer proteins as adoptive T cell vectors (ATVs). The nanoparticle's core is an acid-degradable metal–organic framework (ZIF-8) prepared by the co-precipitation method, loaded with perforin that potently lyses tumor cells and a granzyme B that promotes apoptosis of tumor cells.[2,23] Since perforin and granzyme B are inherent glycoproteins in T cells' lysosomes. These glycoproteins have a high glycosylation level, effectively preventing hydrolase in the lysosome from degrading them.[24,25] Next, calcium ions were deposited on the surface or inside of ZIF-8. The calcium ion or calcium carbonate ($CaCO_3$) induces ZIF-8 mineralization with good biocompatibility and acid degradability, and its degradation product Ca^{2+} enhances the functions of perforin and granzyme B.[26] A CD63 aptamer (CD63-Apt) was modified by biotin on the surface mineralized ZIF-8 to give the LYS-NPs the ability to target cell lysosomes (**Scheme 1**a). Because the lysosome environment is acidic, pH of approximately 5.0, the LYS-NPs can be degraded. The degradation products perforin, granzyme B, and Ca^{2+} stored in the lysosome (Scheme 1b; Movie S1, Supporting Information). When the major histocompatibility complex (MHC) of tumor cells does not activate the T cell receptor (TCR), ATVs remain

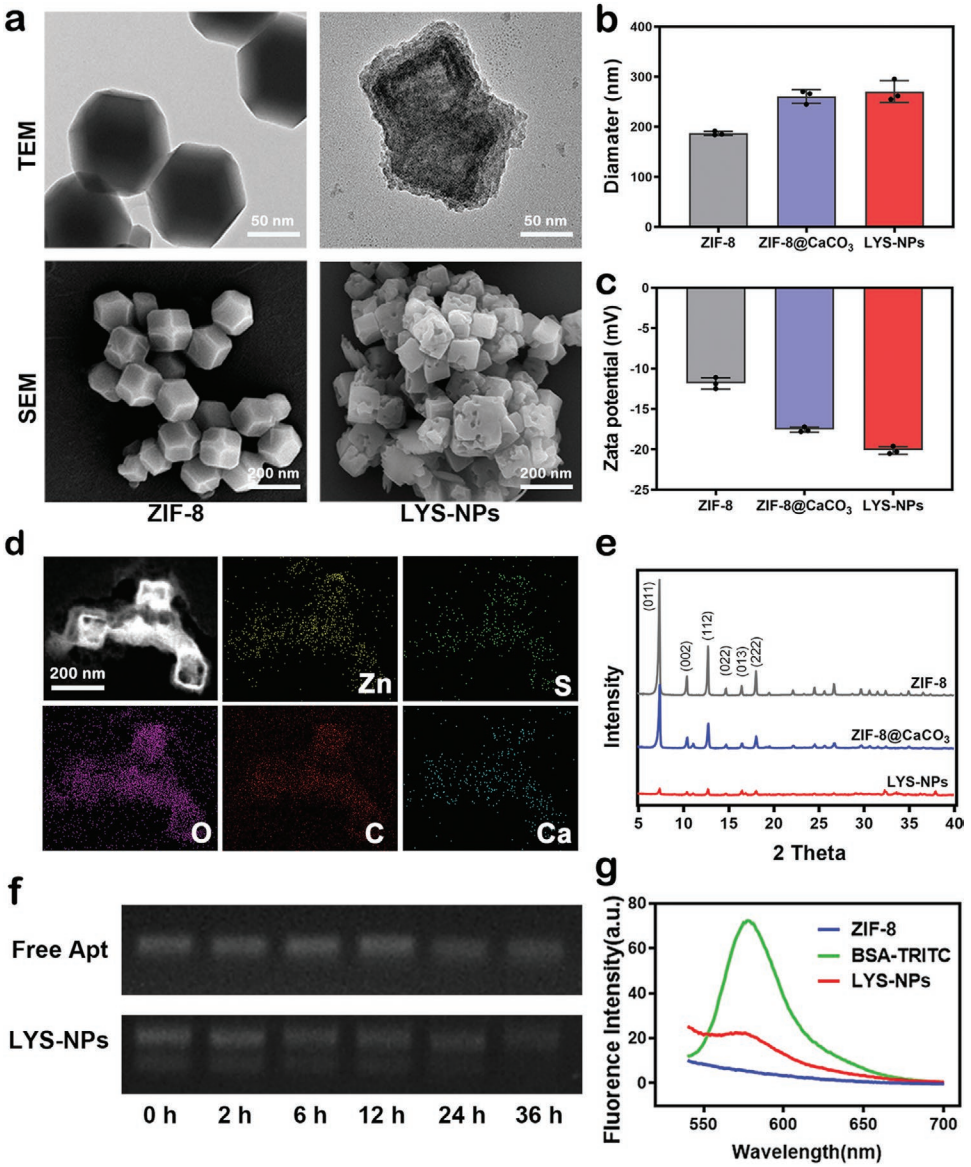

Figure 1. Preparation and characterization of LYS-NPs. a) Morphology assessment of ZIF-8 and LYS-NPs using transmission electron microscopy (TEM) and scanning electron microscopy (SEM). b) DLS measurements of hydrodynamic size (diameter) and c) zeta potential of ZIF-8, ZIF-8@$CaCO_3$, and LYS-NPs. Data presented as mean ± s.d. (n = 3). d) EDS images showing the distribution for the elemental mapping of calcium (cyan), carbon (red), oxygen (purple), zinc(yellow), and sulfur (green). Scale bar: 200 nm. e) The XRD patterns of ZIF-8, ZIF-8@$CaCO_3$, and LYS-NPs, respectively. f) Stability analysis of free Apt and LYS-NPs. Both were stored at 37 °C in 10% FBS medium for a time ranging from 0 to 36 h. g) Fluorescence emission profile of ZIF-8 and LYS-NPs encapsulated with TRITC-BSA.

stable in the lysosome. Oppositely, when the MHC activates the TCR, the lysosome discharges its contents to immunological synapses.[27] Therefore, when ATVs reach the tumor site and are activated by tumor cells, they trigger the autonomously controlled release of perforin, granzyme B, and Ca^{2+} for tumor treatment (Scheme 1c; Movie S1, Supporting Information).

2. Results and Discussion

To confirm that the synthesized LYS-NPs have an ideal structure and function, we first characterized the materials. Through transmission electron microscopy (TEM), LYS-NPs have a mineralized polygonal structure and a relatively uniform layer of calcium carbonate coating visible on the surface of ZIF-8, with a thickness of approximately 25 nm. Combined with scanning electron microscopy (SEM) observations, after the deposition of calcium carbonate, the particles' shape transformed from the original dodecahedron to an approximate cubic structure (**Figure 1**a; Figures S1 and S2, Supporting Information). Dynamic light scattering (DLS) measurements revealed that the nanoparticles' hydrodynamic diameter showed a slight increase after coating. The overall particle size was 270.6 nm, with a reduced zeta potential (Figure 1b,c; Figure S3, Supporting

Information). To verify the correct assembly of the LYS-NPs, we successfully identified the essential elements contained in each layer structure through element mapping analysis. The zinc (Zn) contained in ZIF-8, the sulfur (S) contained in the loaded protein, and calcium (Ca), carbon (C), oxygen (O) of the calcium carbonate shells (Figure 1d). However, no prominent core–shell structure was observed by the element mapping test. Combined with the BET surface area test, LYS-NPs has higher BET surface area and smaller pore size than ZIF-8 itself (Figure S4, Supporting Information). We believe that calcium carbonate is deposited in the outer layer of the ZIF-8 structure and mineralized into it. X-ray diffraction (XRD) (Figure 1e) and Fourier transform infrared (FTIR) spectroscopy analysis (Figure S5, Supporting Information) were used to characterize the structure of LYS-NPs further. The use of tetramethylrhodamine-labeled BSA (BSA-TRITC) provides evidence of protein encapsulation. Precisely, we scanned the fluorescence spectra of the BSA-TRITC-coated nanoparticles, and an emission wavelength of 572 nm was detected, which is consistent with the characteristic peak of TRITC (Figure 1f). We then designed a biotin-conjugated CD63-Apt based on the lysosomal-specific marker CD63, coupling it to the calcium carbonate shell on the nanoparticle's outer layer.[28] To verify the coupling of aptamers through hydrodynamic diameter and zeta potential detection, we found that aptamer coupling increased the nanoparticles' diameter and decreased the zeta potential (Figure 1b,c). Also, the visualization of LYS-NP nucleic acid images verified the successful attachment of the aptamers. Because the protein contained in the serum may bind to the aptamer and interfere with its normal function,[29] we used nucleic acid electrophoresis to detect the stability of aptamers in LYS-NPs stored in a medium under physiological conditions (37°C, 10% FBS). The results showed that the resistance of surface aptamers of LYS-NPs to 10% FBS is at least 36 hours (Figure 1g). To ensure the biological safety of LYS-NPs against ATVs, we evaluated their cytotoxicity. In the process, after 24 hours of incubation with LYS-NPs and T cells, the relative viability of T cells was over 85%, indicating that 2 mg mL^{-1} LYS-NPs and its degradation products had no significant cytotoxicity (Figure S6, Supporting Information). The above LYS-NP characterization and functional results could therefore meet our application requirements. These characterization results indicate that the LYS-NPs are structurally consistent with our design and have ideal stability and biological safety.

We describe the LYS-NP multi-step synthesis process and characterization using ZIF-8 and $CaCO_3$ to produce carrier nanoparticles that can target lysosomes. To verify the initial hypothesis, we demonstrated the necessity of ZIF-8 and $CaCO_3$ in the synthesis through protein encapsulation rate, leakage rate, and stability testing. Using the BCA method to measure the nanoparticles' albumin concentration, the drug encapsulation rate of LYS-NPs reached 71.36% (**Figure 2**a), higher than $CaCO_3$ alone. Also, we evaluated the kinetic curve of LYS-NPs dissolution at different pH values and the accompanying protein release. Among the values, pH 5.0 is similar to the pH of the intracellular lysosomal environment. Within 4 hours, nearly 100% of calcium carbonate is dissolved. The experimental results also showed that LYS-NPs still had 74.0% calcium retained when stored in a pH 7.4 solution for one hour, and 68.8% calcium remained after 4 hours (Figure 2b; Figure S7, Supporting Information). Even if a small number of calcium ions are lost during the journey, flow cytometry results can prove that LYS-NPs can successfully transport many of the calcium ions into the cells (Figure S8, Supporting Information). We observed that the levels of calcium ions released by the degradation of calcium carbonate and protein released by the structural collapse of ZIF-8 increased almost simultaneously (Figure 2b; Figure S9, Supporting Information). This observation indicates that the ZIF-8 structure and calcium carbonate shell of LYS-NPs have ideal acid sensitivity characteristics and exhibit pH- and time-dependent Ca2+ and protein release patterns. TEM images can intuitively reflect the process of LYS-NPs disintegrating gradually over time. In the environment at pH = 6.3, the outer layer of LYS-NPs was partially dissolved and became rounded after 15 min. The main components of LYS-NPs were mostly dissolved within 30 min and were dispersed into several small particles; after 45 min, only a few particles had not yet completely dissolved (Figure S10, Supporting Information). We noticed that when the pH = 7.4, calcium carbonate is partially dissolved even after a long time, but the protein is rarely released. This result may occur because the ZIF-8 material did not degrade in a neutral environment.[22] This characteristic also makes the material exhibit a specific protective effect on internal proteins. We confirmed that the loss rate of protein in LYS-NPs did not exceed 5% in the PBS storage environment for up to 7 days, much lower than using ZIF-8 or $CaCO_3$ alone (Figure 2c). As we know, ZIF-8 alone can directly encapsulate proteins into the framework through the connection of MIM and Zn^{2+} bridging units. Although this method has high encapsulation efficiency and strong stability,[20,21] the mineralized ZIF-8 (ZIF-8 with $CaCO_3$) seems to have more advantages, especially in transportation. Compared to "backpack" technology connecting nanomaterials to T cells' surface, reassembling of the lysosomes may avoid the loss of backpacks or the inactivation of drugs during the complicated delivery process in vivo. We have not confirmed this.

To further confirm that LYS-NPs could successfully load proteins into T-cell lysosomes, we performed the targeting ability and acid degradability of the LYS-NPs. To verify the ability of LYS-NPs coupled with CD63-Apt to target lysosomes, we also designed random-order aptamer (Random-Apt)-coupled nanoparticles and nanoparticles without any aptamers to serve as a control. Among them, CD63-Apt could specifically bind to lysosomes, while random-order aptamers only consist of a random nucleotide sequence that does not have a targeting function. The three nanoparticles were all loaded with BSA-TRITC fluorescent protein. After cocultivation with T cells for 4 h, the observation by fluorescence confocal microscopy revealed that the three groups of fluorescent proteins all entered T cells to varying degrees. It is worth noting that the CD63-Apt group exhibited the most robust targeting ability, showing the best coincidence of red fluorescence (BSA-TRITC) and green fluorescence (lysosome). In contrast, the Random-Apt group and the pure nanoparticle group only had partial protein entry, with limited fluorescence coincidence observed (Figure 2d; Figures S11 and S12, Supporting Information). These nontargeted lysosomal affinity phenomena are due to the nonspecific endocytosis of nanoparticles or lysosomes' defense mechanism

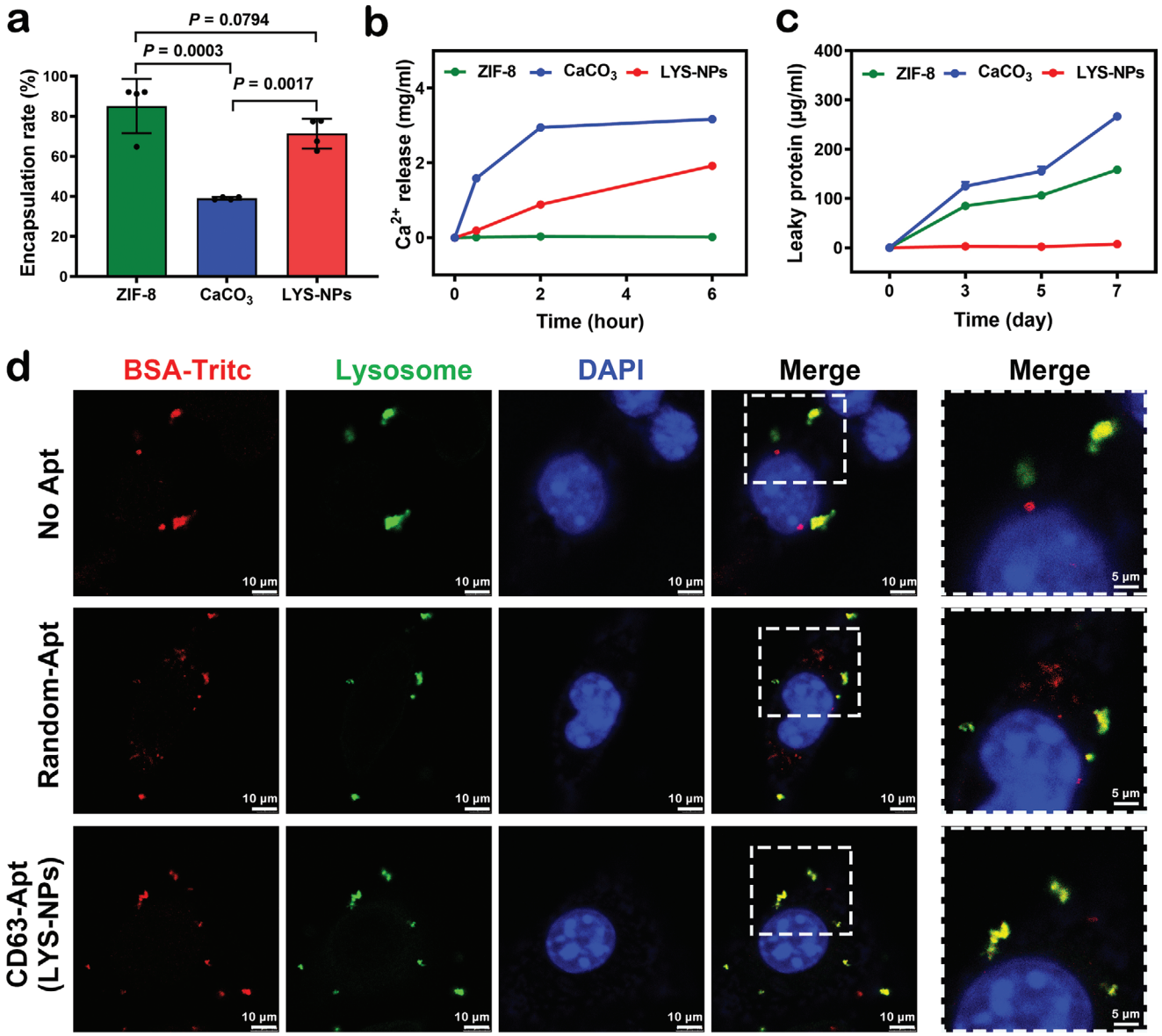

Figure 2. LYS-NPs with lysosomal targeting and pH sensitivity to release drugs and calcium ions. a) Protein encapsulation rate of three different nanomaterials. b) Calcium-ion release curve of the nanomaterials at pH = 7.4. c) The protein leakage curve of the nanomaterials at pH = 7.4. d) Confocal fluorescence microscopy images to monitor the uptake of LYS-NPs by 4T1 cells. The cells were lysosome stained with daylight 488 (green) and nuclei were stained with DAPI (blue). TRITC-labeled BSA (red) was encapsulated into nanoparticles, and they were incubated with T cells. The merged images show the internalization of the LYS-NPs inside the cell lysosome.

against foreign bodies.[30] Also, the median fluorescence index (MFI) of BSA-TRITC inside the cells was detected by flow cytometry. We found that the nanoparticles' MFI connected with the CD63-Apt and Random-Apt groups was significantly higher than that of the pure nanoparticle group. Still, there was no difference between the two (Figure S13, Supporting Information). We also investigated the fluorescent perforin and granzyme B weather work in this process and got a similar result to fluorescently labeled BSA (Figure S14, Supporting Information). This result indicated that the attachment of the aptamer increases the affinity of the material with the cells, allowing cells that do not initially possess phagocytic functions to internalize more nanoparticles.

Next, we envisaged that the use of dendritic cell (DC) antigen processing and presentation of mouse breast cancer cell lysates could prepare breast cancer-specific ATVs. The inspiration for this design comes from recent developments in immune cell membrane display technology. The primary purpose is to enhance the function of specific receptors and cell functions on the surface of immune cells by pretreatment of immune cells, resulting in an enhanced immunotherapy effect on diseases.[31,32] This concept is similar to CAR-T therapy in tumor immunotherapy.[33] In this application, we constructed ATVs with memory for tumor cells. In detail, the antigen information of tumor lysates processed by DCs is presented to $CD8^+$ T cells.[34] (**Figure 3**a) To test our hypothesis, we first

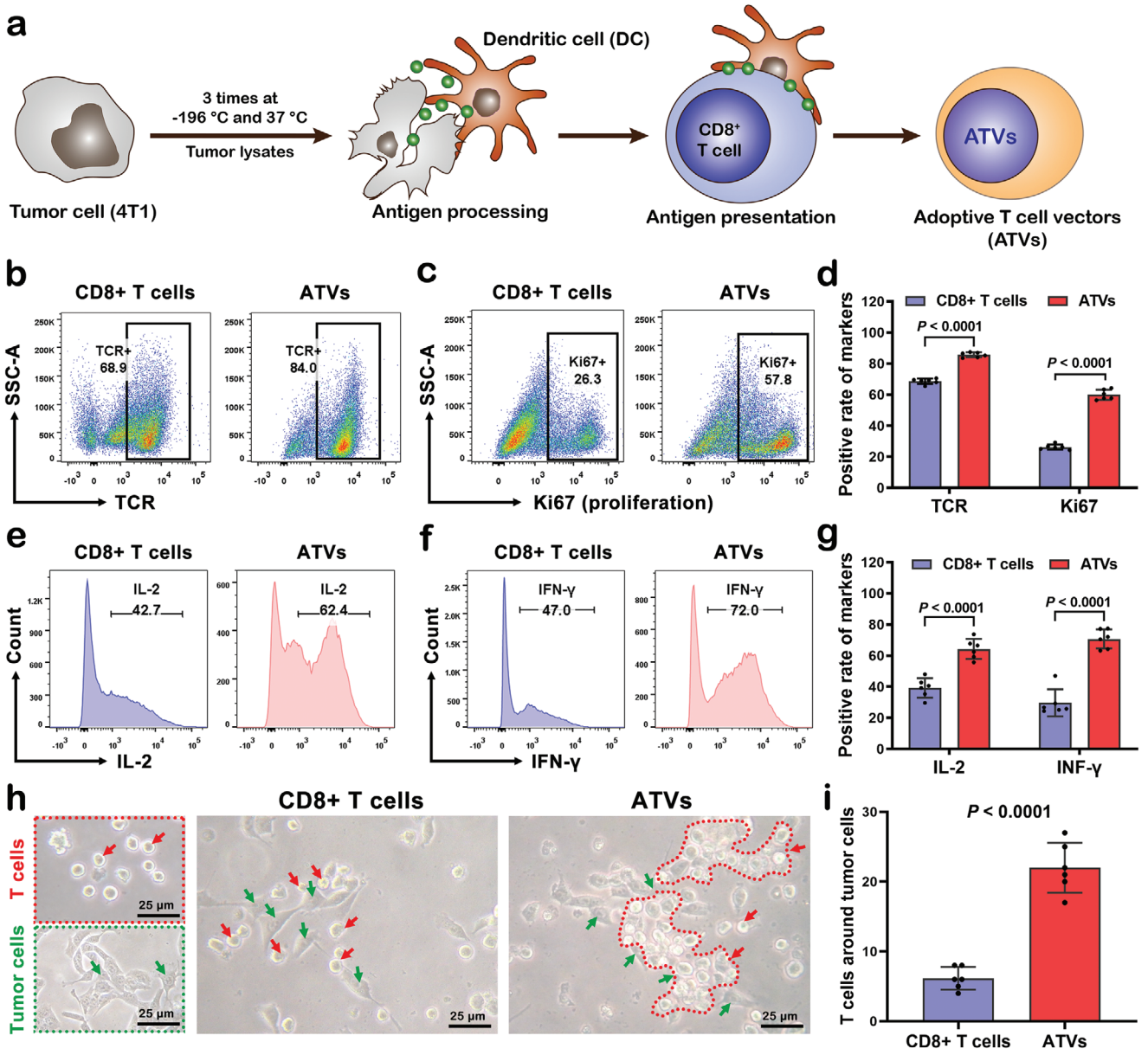

Figure 3. Preparation of adoptive T cell vectors (ATVs) for tumor cells (breast cancer). a) Schematic of forming ATVs. The antigen information of tumor lysates was first processed by DCs and then presented to $CD8^+$ T cells. b–d) Flow cytometry analysis of T cell ability to recognize antigens and proliferate. e–g) Flow cytometry analysis of T cell function. h) Representative Images showing $CD8^+$T cells or ATVs interacting with tumor cells at 200× magnification, and i) the quantification of T cell numbers around the tumor cells is given. Data in (d,g,i) are expressed as the mean ± s.d., (n = 6), unpaired two-tailed t-test.

stimulated DCs with lysates from mouse breast cancer cells. Flow cytometry detected a higher expression level of histocompatibility complex MHC and costimulatory molecule CD86 on the surface of DCs cells after stimulation (Figure S15, Supporting Information), which is the basis for antigen presentation to activate T cells.[35] In addition, real-time polymerase chain reaction (PCR) confirmed that the expression of both MHC and CD86 mRNA was upregulated (Figure S16, Supporting Information). Furthermore, we cocultured $CD8^+$ T cells sorted in mice with the above two groups of DCs to obtain ATVs specific for breast cancer. To verify the effectiveness and specificity of the T cell vectors, we detected the TCR and Ki67 expression in the two groups of T cell vectors by flow cytometry. We found that the ATVs presented by the antigen expressed higher TCR and Ki67 levels (Figure 3b–d), indicating that it has stronger tumor cell recognition ability[36] and proliferation ability.[37,38] At the same time, ATVs secrete more IL-2 and IFN-γ (Figure 3e–g), representing a manifestation of T cell effector activation.[39,40] The ATVs obtained by our pretreatment method have a strong tumor cell activation effect and binding ability, which is related to the high expression of TCR after treatment. TCR is a key receptor for $CD8^+$ effector and memory T cells and is activated by MHC on the surface of tumor cells.[41–43] We used dendritic cells to present breast tumor antigens to $CD8^+$

T cells in advance to produce ATVs. In theory, ATVs have a strong specific recognition and binding ability for breast cancer cells. To verify this concept, we cocultured two sets of T cells (ATVs and $CD8^+$ T cells) with breast cancer cells and observed the combination of the two cells with a light microscope. As a suspension cell, the round-shaped T cells should be free flowing in the culture medium, while the breast cancer cells are spindle-shaped adherent cells. After two days of cocultivation, the control group had only a small number of $CD8^+$ T cells combined with breast cancer cells. In contrast, ATVs attach to breast cancer cells at high density and lose suspension fluidity (Figure 3h,i). Moreover, cell apoptosis test confirmed that ATVs have a stronger ability to kill breast cancer cells than $CD8^+$ T cells that are not stimulated by DC (Figure S17, Supporting Information). Since we store anticancer drugs in lysosomes of T cells, their efflux is achieved through the activation of TCR.[27] As well known, TCR-controlled lysosome efflux can release perforin and granzyme B to immunological synapses, which is the ideal functional site of immunotherapy. Although the method of artificial controlled release of drugs can achieve regional drug release, the release of a large amount of drugs in inefficient surrounding areas may lead to off-target secondary drug effects.[44–46] Otherwise, to verify whether the protein-loaded into T cells will be released without stimulation by cancer cells, we performed and found that only a small amount of protein in the lysosome was released without the stimulus. This phenomenon of unstimulated protein release may be due to cell culture for a period that triggered non-TCR-dependent apoptosis.[47,48] The release rate of the cytotoxic protein in T cells for 48 hours' culture was 31.0%, while the release rate after interacting with tumor cells was 77.1% (Figure S18, Supporting Information). This indicates that cancer cells play a key role in initiating the release of loaded protein in T cells. Overall, ATVs pretreated with specific antigens have stronger specificity for cancer cells. The ATVs can bind to cancer cells and release drugs, making them ideal LYS-NP delivery vehicles.

To determine whether the LYS-NPs carried by ATVs can effectively release anticancer drugs and induce cancer cell apoptosis, we constructed a coculture system with breast cancer cells in vitro.[49] We compared the assembly of ATVs and LYS-NPs (ATVs@LYS-NPs) with LYS-NPs alone and ATVs as controls. After coculturing with breast cancer cells for 24 h, the fluorescence of cancer cells after perforin and granzyme B uptake was observed. The appearance of perforin and granzyme B partly originated from the release of T cells themselves,[50] with the other part originating from the degradation of LYS-NPs. Confocal image observation revealed that the surface area of breast cancer cells cocultured with ATVs@LYS-NPs contained a large amount of perforin and granzyme B, much higher than that with the use of LYS-NPs or ATVs alone (**Figure 4**a,c,d; Figure S19, Supporting Information). The flow cytometry results also showed the same trend, proving that ATVs@LYS-NPs enhanced the quantity of perforin and granzyme B in breast cancer cells (Figure 4b,e,f). We found that there was also a certain amount of drug intake when LYS-NPs were used alone, which may be due to the transmembrane effect or endocytosis of nanoparticles in the tumor cell environment.[51] For the therapeutic effect, treatment with ATVs@LYS-NPs caused 35.4% tumor cell apoptosis, which was increased by 2.3 times or 1.2 times, respectively, compared with LYS-NPs or ATVs alone, confirming an enhanced antitumor ability (Figure 4g,h). At the same time, it is also much higher than stimulated with protein-encapsulated ZIF-8 or $CaCO_3$ materials (Figure S20, Supporting Information). The application of LYS-NPs alone also allowed their entry into tumor cells, though no significant effect was observed. This result may be due to the degradation products of LYS-NPs in tumor cell lysosomes, which are not inducers of lysosomal autophagy or apoptosis, although lysosomes are the targets of many cancer treatments.[52,53]

To investigate whether ATVs@LYS-NPs could achieve immunotherapy for breast cancer, we used a tumor-bearing model of the same strain of breast cancer. 4T1 breast cancer cells were injected into the bilateral breast fat pads of BALB/c mice. Seven days after injection, saline, ATVs@LYS-NPs, $CD8^+$ T cells, and ATVs labeled with DiR iodide crimson fluorescent probe were injected through the tail vein for treatment. Those stained cells or vectors were visually imaged in mice the next day, and there was significant red fluorescence enrichment in the breast-cancer-tumor-bearing parts of mice treated with ATVs@LYS-NPs and ATVs alone (**Figure 5**a). It was confirmed that ATVs could be used as ideal tumor-targeting carriers in vivo. Since our method of preparing ATVs is based on the traditional process of preparing adoptive T cells. In the current experimental research and clinical application, this method is mature and can ensure the survival of T cells in mammals for more than 3 weeks.[54] Moreover, in the experiment, we can still detect the strong fluorescence signal of ATVs in the tumor area after 3 weeks after injection of ATVs in mice (data not shown). Also, the material we designed (LYS-NP) has no apparent cytotoxicity to ATVs. In summary, we have reason to believe that the ATVs we prepared can survive in vivo for up to 3 weeks. We found that in addition to the tumor-bearing parts of mice, red fluorescence appeared in the internal organs such as the liver and spleen. This result is related to the characteristics of T cells as the critical cells of the immune system in the body. The liver and spleen are essential organs and are rich in immune cells.[55] Theoretically, ATVs only bind to tumor cells to activate drug release from lysosomes in vivo, but their enrichment in other organs may cause unexpected drug release or organ damage. Therefore, we evaluated the systemic impact of the application of ATVs@LYS-NPs by H&E staining of the organs of each group. No obvious lesions were observed in the heart, liver, spleen, lung or kidney of the mice (Figure S21, Supporting Information). By conducting routine blood tests to further assess the health status of mice, we found that their main cell contents (RBC, WBC, Lymph, Gran) were well within normal ranges (Table S1, Supporting Information). The hemolysis test also showed that the NPs have no apparent toxicity (Figure S22, Supporting Information). Based on histological and hematological analyses, it was demonstrated that the in vivo application of ATVs@LYS-NPs has high biological safety. To further confirm the effect of in vivo cancer treatment, we showed that the ATVs@LYS-NPs treatment obviously hindered the growth of the tumor based on tumor volume measurement and tumor body photographs, and the tumor suppression rate reached 70.9% in 30 days. The inhibition rate of pure ATVs was only approximately 26.9% (Figure 5b,c; Figures S23 and S24, Supporting Information). The application of ATVs@LYS-NPs also significantly increased

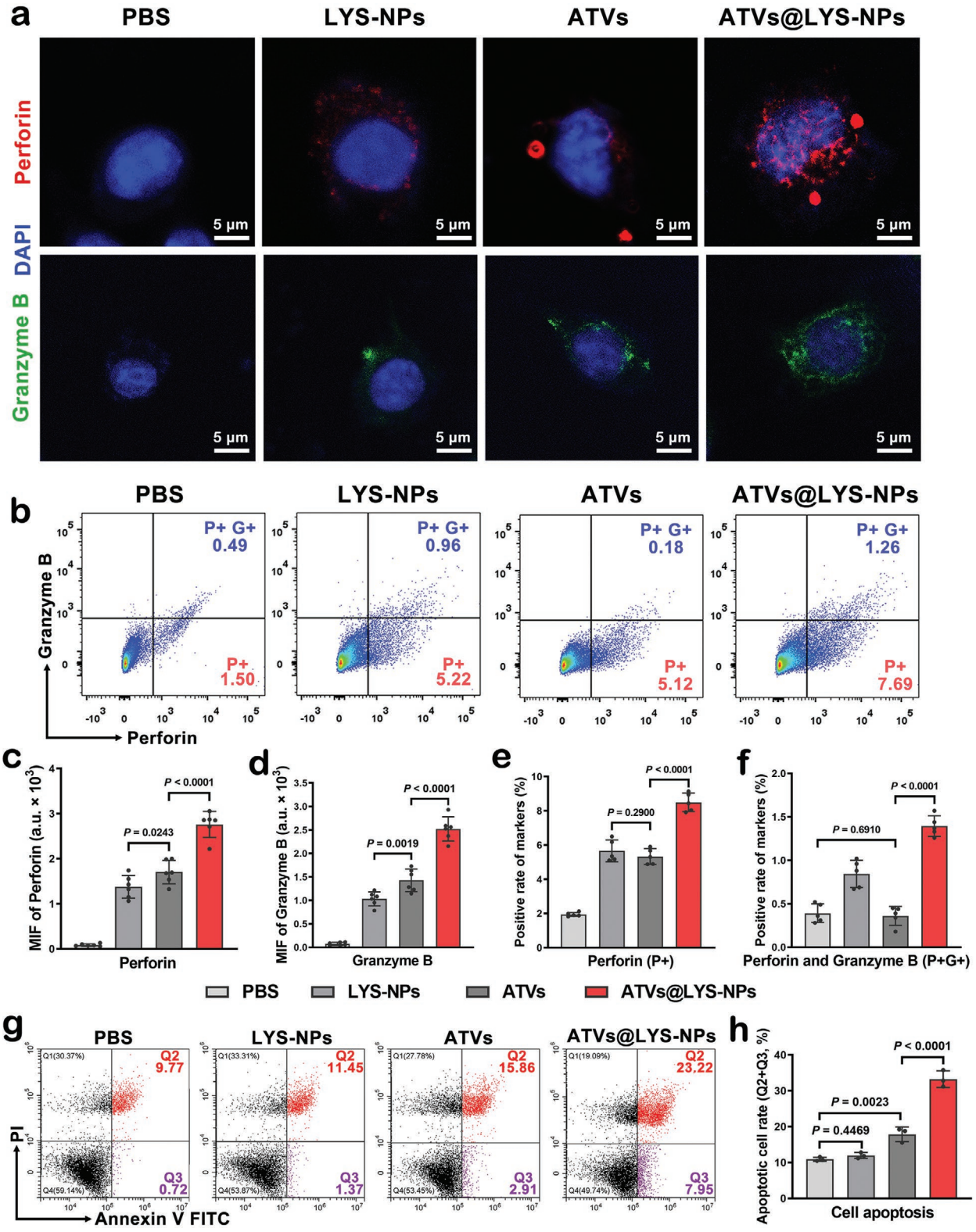

Figure 4. ATV@LYS-NPs targeted delivery of perforin and granzyme B to promote tumor cells apoptosis. a) Confocal fluorescence imaging of drug (perforin and granzyme B) entering in 4T1 cells (red = perforin, green = granzyme B, blue = nuclei; scale bars = 5 μm). b) Flow cytometry analysis of the amount of active protein inside 4T1 cells using different treatment. c,d) The mean fluorescence intensity (MFI) in confocal fluorescence imaging was measured and analyzed. e,f) Quantitative analysis of the positive rate of cells containing perforin and granzyme B is given. g) After incubation with PBS, LYS-NPs, ATVs, and ATVs@LYS-NPs for 24 h, flow cytometry analysis of 4T1 cells apoptosis level is shown, and the quantification of apoptosis rates is presented in (h). Data are presented as mean ± s.d. (c–f, $n = 6$; h, $n = 3$), one-way analysis of variance (ANOVA) with Tukey's multiple comparison test.

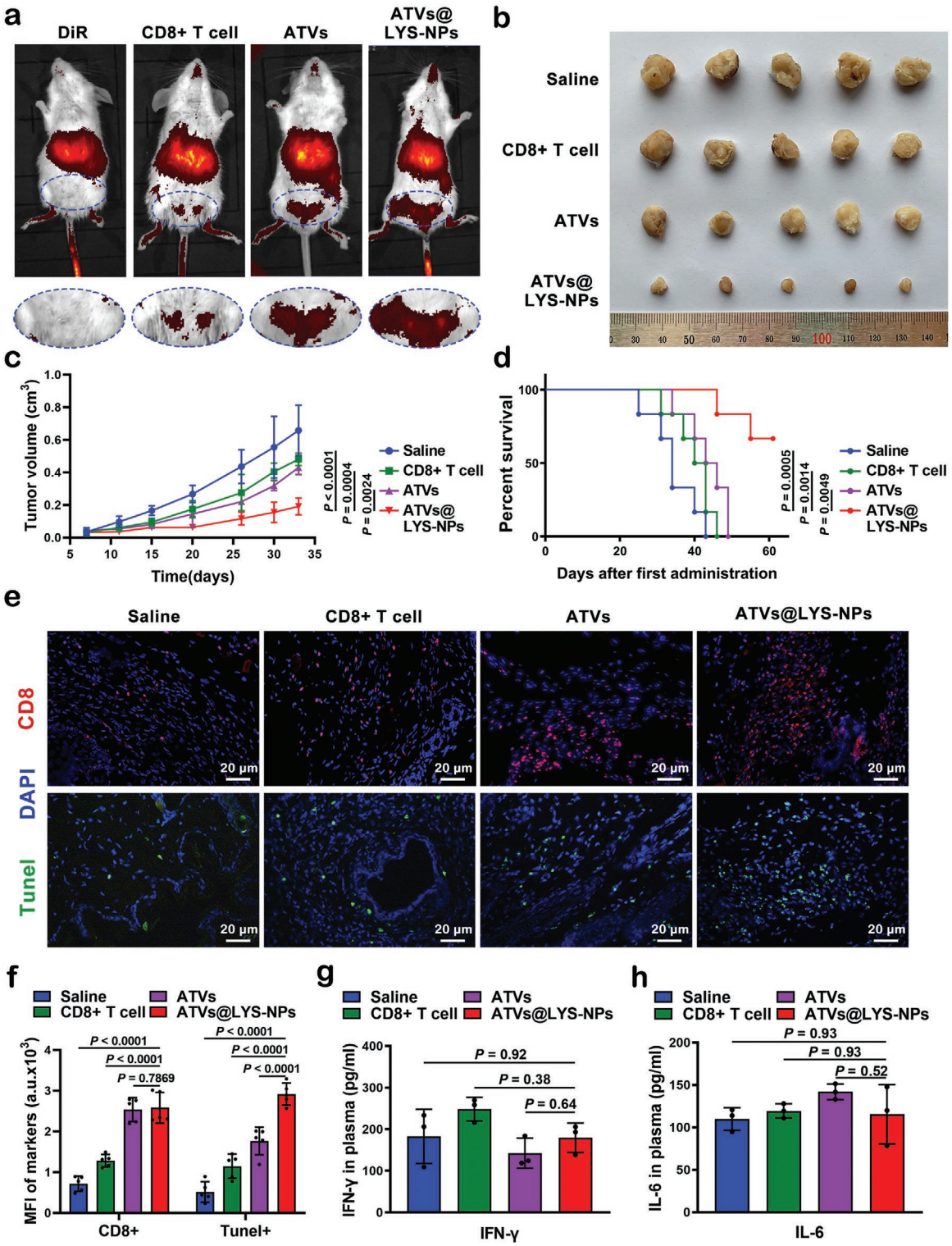

Figure 5. Targeted drug delivery and antitumor effect of ATVs@LYS-NPs in vivo. a) Fluorescence images of mice injected with: 1) saline+DiR, 2) $CD8^+$T cells, 3) ATVs, 4) ATVs@LYS-NPs. T-cell migration at a region of interest (ROI, highlighted with blue circles) is shown. b) The images of tumors. c) The profiles of tumor volumes variation. Data are presented as mean ± s.d. ($n = 5$). d) Survival curves of mice receiving different treatments ($n = 6$). e) Terminal deoxynucleotidyl transferase dUTP nick end labeling (TUNEL) staining (green) and CD8 staining (red) of tumor sections were observed by fluorescence microscopy. Cell nuclei were stained with DAPI (blue). Scale bars: 20 μm. f) MFI was measured and analyzed. Data presented as mean ± s.d. ($n = 6$), one-way ANOVA with Tukey's multiple comparison test. g,h) enzyme-linked immunosorbent assay (ELISA) of plasma IFN-γ and IL-6 concentration in 4T1-tumor-bearing mice after different treatment. Data are presented as mean ± s.d. ($n = 3$), one-way ANOVA with Tukey's multiple comparison test.

the survival time of tumor-bearing mice (Figure 5d). Focusing on local tissue, compared with mice treated with vehicle alone, mice treated with ATVs@LYS-NPs showed more $CD8^+$ T cell recruitment and more cancer cell apoptosis in tumor areas (Figure 5e,f; Figure S25, Supporting Information). Although the therapeutic effect observed in this challenging tumor model was modest, this was the effect that can be achieved with one injection, indicating that the method was expected to improve the treatment effect after repeated administration.[56] To further address whether ATVs@LYS-NPs can trigger systemic immune cell activation, we evaluated the antitumor cytokines interferon-gamma (IFN-γ) and interleukin 6 (IL-6). We found that the peripheral blood IFN-γ and IL-6 levels in the ATVs@LYS-NP treatment group were not significantly different from those in the other treatment groups (Figure 5g,h). This finding suggests that the application of experimental doses of ATVs@LYS-NPs is within a safe range. These data demonstrate that ATVs@LYS-NPs show superior tumor-targeted drug delivery ability and promote tumor cell apoptosis in tumor immunotherapy, suggesting that this formulation has certain antitumor activity and biological safety.

3. Conclusion

We have developed reprogrammed $CD8^+$ T Cells by lysosome-targeting LYS-NPs to improve cancer immunotherapy. We have shown that LYS-NPs store perforin and granzyme B in the lysosomes of ATVs and the therapeutic proteins are released when the TCR of ATVs binds to tumor cells. Meanwhile, $CaCO_3$ is degraded into Ca^{2+} in the lysosome, which can synergistically enhance the effects of perforin and granzyme B. These three elements possess the powerful ability to induce cell apoptosis and promote target cell lysis in immunological synapses.[57] Importantly, LYS-NPs reprogramming lysosomes of $CD8^+$ T cells solves the major problems faced by anti-solid-tumor strategies, namely, the insufficient targeting of T cells to the tumor area, and the sharp decline in the synthesis and release of cytotoxic proteins. Our work, constructing a "super-cytotoxic T lymphocyte" for targeting tumors and releasing cytotoxic proteins, has opened up new horizons for anti-solid-tumor-strategies by immunological methods.

Supporting Information

Supporting Information is available from the Wiley Online Library or from the author.

Acknowledgements

Q.Z. and Z.G. contributed equally to this work. This work was supported by the National Key R&D Program of China (2018YFC1105300); the National Natural Science Foundation of China (81771050, 81700931); the Special Fund for Technical Innovation of Hubei Province (2017AHB046); and the Natural Science Foundation of Hubei Province (2017CFA025). The authors would like to thank Qian Wu (Department of Stomatology, Maternal and Child Hospital of Hubei Province) for animation as well as Chenhui Ji (College of Chemistry and Molecular Sciences, Wuhan University) for the assistance with material synthesis. The authors also thank Yan Wang (the Center for Instrumental Analysis and Metrology, Institute of Hydrobiology, Chinese Academy of Science) for technical assistance in in vivo imaging system. All animal experiments were approved by the Ethics Committee of Wuhan University (ethical approval number 69/2017). The animal experiment process complied with all relevant ethics.

Conflict of Interest

The authors declare no conflict of interest.

Data Availability Statement

Research data are not shared.

Keywords

adoptive T cells, cancer therapy, immunotherapy, lysosomes, metal–organic frameworks

Received: January 24, 2021
Revised: February 24, 2021
Published online: March 24, 2021

[1] C. Yee, *Curr. Opin. Immunol.* **2018**, *51*, 197.
[2] I. Voskoboinik, J. C. Whisstock, J. A. Trapani, *Nat. Rev. Immunol.* **2015**, *15*, 388.
[3] M. L. Dustin, E. O. Long, *Immunol. Rev.* **2010**, *235*, 24.
[4] H. Wang, D. J. Mooney, *Nat. Mater.* **2018**, *17*, 761.
[5] J. Xue, Z. Zhao, L. Zhang, L. Xue, S. Shen, Y. Wen, Z. Wei, L. Wang, L. Kong, H. Sun, Q. Ping, R. Mo, C. Zhang, *Nat. Nanotechnol.* **2017**, *12*, 692.
[6] N. A. Hotaling, L. Tang, D. J. Irvine, J. E. Babensee, *Annu. Rev. Biomed. Eng.* **2015**, *17*, 317.
[7] J. Conniot, A. Scomparin, C. Peres, E. Yeini, S. Pozzi, A. I. Matos, R. Kleiner, L. I. F. Moura, E. Zupančič, A. S. Viana, H. Doron, P. M. P. Gois, N. Erez, S. Jung, R. Satchi-Fainaro, H. F. Florindo, *Nat. Nanotechnol.* **2019**, *14*, 891.
[8] M. S. Goldberg, *Nat. Rev. Cancer* **2019**, *19*, 587.
[9] Z. S. Dunn, J. Mac, P. Wang, *Biomaterials* **2019**, *217*, 119265.
[10] N. Siriwon, Y. J. Kim, E. Siegler, X. Chen, J. A. Rohrs, Y. Liu, P. Wang, *Cancer Immunol. Res.* **2018**, *6*, 812.
[11] T. T. Smith, S. B. Stephan, H. F. Moffett, L. E. McKnight, W. Ji, D. Reiman, E. Bonagofski, M. E. Wohlfahrt, S. P. S. Pillai, M. T. Stephan, *Nat. Nanotechnol.* **2017**, *12*, 813.
[12] M. T. Stephan, J. J. Moon, S. H. Um, A. Bershteyn, D. J. Irvine, *Nat. Med.* **2010**, *16*, 1035.
[13] L. Tang, Y. Zheng, M. B. Melo, L. Mabardi, A. P. Castaño, Y. Q. Xie, N. Li, S. B. Kudchodkar, H. C. Wong, E. K. Jeng, M. V. Maus, D. J. Irvine, *Nat. Biotechnol.* **2018**, *36*, 707.
[14] M. T. Stephan, S. B. Stephan, P. Bak, J. Chen, D. J. Irvine, *Biomaterials* **2012**, *33*, 5776.
[15] B. Huang, W. D. Abraham, Y. Zheng, S. C. Bustamante López, S. S. Luo, D. J. Irvine, *Sci. Transl. Med.* **2015**, *7*, 291ra94.
[16] N. K. Maddigan, A. Tarzia, D. M. Huang, C. J. Sumby, S. G. Bell, P. Falcaro, C. J. Doonan, *Chem. Sci.* **2018**, *9*, 4217.
[17] F. Lyu, Y. Zhang, R. N. Zare, J. Ge, Z. Liu, *Nano Lett.* **2014**, *14*, 5761.
[18] G. Chen, S. Huang, X. Kou, S. Wei, S. Huang, S. Jiang, J. Shen, F. Zhu, G. Ouyang, *Angew. Chem., Int. Ed.* **2019**, *58*, 1463.
[19] D. Giliopoulos, A. Zamboulis, D. Giannakoudakis, D. Bikiaris, K. Triantafyllidis, *Molecules* **2020**, *25*, 185.

[20] W. Liang, P. Wied, F. Carraro, C. J. Sumby, B. Nidetzky, C. K. Tsung, P. Falcaro, C. J. Doonan, *Chem. Rev.* **2021**, *121*, 1077.
[21] S. S. Nadar, L. Vaidya, V. K. Rathod, *Int. J. Biol. Macromol.* **2020**, *149*, 861.
[22] T. T. Chen, J. T. Yi, Y. Y. Zhao, X. Chu, *J. Am. Chem. Soc.* **2018**, *140*, 9912.
[23] J. A. Trapani, M. J. Smyth, *Nat. Rev. Immunol.* **2002**, *2*, 735.
[24] A. J. Brennan, J. Chia, K. A. Browne, A. Ciccone, S. Ellis, J. A. Lopez, O. Susanto, S. Verschoor, H. Yagita, J. C. Whisstock, J. A. Trapani, I. Voskoboinik, *Immunity* **2011**, *34*, 879.
[25] M. D. Prakash, C. H. Bird, P. I. Bird, *Immunol. Cell Biol.* **2009**, *87*, 249.
[26] J. A. Lopez, O. Susanto, M. R. Jenkins, N. Lukoyanova, V. R. Sutton, R. H. Law, A. Johnston, C. H. Bird, P. I. Bird, J. C. Whisstock, J. A. Trapani, H. R. Saibil, I. Voskoboinik, *Blood* **2013**, *121*, 2659.
[27] A. Durgeau, Y. Virk, S. Corgnac, F. Mami-Chouaib, *Front. Immunol.* **2018**, *9*, 14.
[28] C. Zhou, T. Chen, C. Wu, G. Zhu, L. Qiu, C. Cui, W. Hou, W. Tan, *Chem. - Asian J.* **2015**, *10*, 166.
[29] W. Ma, Y. Zhan, Y. Zhang, X. Shao, X. Xie, C. Mao, W. Cui, Q. Li, J. Shi, J. Li, C. Fan, Y. Lin, *Nano Lett.* **2019**, *19*, 4505.
[30] C. Orellana-Tavra, S. A. Mercado, D. Fairen-Jimenez, *Adv. Healthcare Mater.* **2016**, *5*, 2261.
[31] M. Shi, P. Zhang, Q. Zhao, K. Shen, Y. Qiu, Y. Xiao, Q. Yuan, Y. Zhang, *Small* **2020**, *16*, 1905185.
[32] P. Zhang, Q. Zhao, M. Shi, C. Yin, Z. Zhao, K. Shen, Y. Qiu, Y. Xiao, Y. Zhao, X. Yang, Y. Zhang, *Nano Lett.* **2020**, *20*, 261.
[33] K. T. Roybal, W. A. Lim, *Annu. Rev. Immunol.* **2017**, *35*, 229.
[34] Y. G. Wu, G. Z. Wu, L. Wang, Y. Y. Zhang, Z. Li, D. C. Li, *Med. Oncol.* **2010**, *27*, 736.
[35] Y. Tomita, E. Watanabe, M. Shimizu, Y. Negishi, Y. Kondo, H. Takahashi, *Cancer Immunol., Immunother.* **2019**, *68*, 1605.
[36] H. Huang, M. J. Sikora, S. Islam, R. R. Chowdhury, Y. H. Chien, T. J. Scriba, M. M. Davis, L. M. Steinmetz, *Proc. Natl. Acad. Sci. USA* **2019**, *116*, 8995.
[37] X. Wang, H. Shen, Q. He, W. Tian, A. Xia, X. J. Lu, *J. Med. Genet.* **2019**, *56*, 29.
[38] X. Wang, Q. He, H. Shen, X. J. Lu, B. Sun, *J. Med. Genet.* **2019**, *56*, 18.
[39] R. Spolski, P. Li, W. J. Leonard, *Nat. Rev. Immunol.* **2018**, *18*, 648.
[40] S. I. Tsukumo, K. Yasutomo, *Front. Immunol.* **2018**, *9*, 101.
[41] J. Kisielow, F. J. Obermair, M. Kopf, *Nat. Immunol.* **2019**, *20*, 652.
[42] J. P. Snook, C. Kim, M. A. Williams, *Sci. Immunol.* **2018**, *3*, eaas9103.
[43] R. O. Emerson, W. S. DeWitt, M. Vignali, J. Gravley, J. K. Hu, E. J. Osborne, C. Desmarais, M. Klinger, C. S. Carlson, J. A. Hansen, M. Rieder, H. S. Robins, *Nat. Genet.* **2017**, *49*, 659.
[44] T. T. Smith, H. F. Moffett, S. B. Stephan, C. F. Opel, A. G. Dumigan, X. Jiang, V. G. Pillarisetty, S. P. S. Pillai, K. D. Wittrup, M. T. Stephan, *J. Clin. Invest.* **2017**, *127*, 2176.
[45] E. D'Ippolito, K. Schober, M. Nauerth, D. H. Busch, *Cancer Immunol., Immunother.* **2019**, *68*, 1701.
[46] B. Wang, B. J. DeKosky, M. R. Timm, J. Lee, E. Normandin, J. Misasi, R. Kong, J. R. McDaniel, G. Delidakis, K. E. Leigh, T. Niezold, C. W. Choi, E. G. Viox, A. Fahad, A. Cagigi, A. Ploquin, K. Leung, E. S. Yang, W. P. Kong, W. N. Voss, A. G. Schmidt, M. A. Moody, D. R. Ambrozak, A. R. Henry, F. Laboune, J. E. Ledgerwood, B. S. Graham, M. Connors, D. C. Douek, N. J. Sullivan, A. D. Ellington, J. R. Mascola, G. Georgiou, *Nat. Biotechnol.* **2018**, *36*, 152.
[47] G. de Saint Basile, G. Ménasché, A. Fischer, *Nat. Rev. Immunol.* **2010**, *10*, 568.
[48] Z. Chen, J. Wang, W. Sun, E. Archibong, A. R. Kahkoska, X. Zhang, Y. Lu, F. S. Ligler, J. B. Buse, Z. Gu, *Nat. Chem. Biol.* **2018**, *14*, 86.
[49] C. S. Chiang, Y. J. Lin, R. Lee, Y. H. Lai, H. W. Cheng, C. H. Hsieh, W. C. Shyu, S. Y. Chen, *Nat. Nanotechnol.* **2018**, *13*, 746.
[50] P. Golstein, G. M. Griffiths, *Nat. Rev. Immunol.* **2018**, *18*, 527.
[51] M. Durymanov, C. Kroll, A. Permyakova, J. Reineke, *Mol. Pharmaceutics* **2019**, *16*, 1074.
[52] Y. Du, P. Peng, T. Li, *ACS Nano* **2019**, *13*, 5778.
[53] C. G. Towers, A. Thorburn, *Cancer Discovery* **2017**, *7*, 1218.
[54] A. E. Foster, A. Mahendravada, N. P. Shinners, W. C. Chang, J. Crisostomo, A. Lu, M. Khalil, E. Morschl, J. L. Shaw, S. Saha, M. T. Duong, M. R. Collinson-Pautz, D. L. Torres, T. Rodriguez, T. Pentcheva-Hoang, J. H. Bayle, K. M. Slawin, D. M. Spencer, *Mol. Ther.* **2017**, *25*, 2176.
[55] C. Zheng, L. Zheng, J. K. Yoo, H. Guo, Y. Zhang, X. Guo, B. Kang, R. Hu, J. Y. Huang, Q. Zhang, Z. Liu, M. Dong, X. Hu, W. Ouyang, J. Peng, Z. Zhang, *Cell* **2017**, *169*, 1342.
[56] Y. Zheng, L. Tang, L. Mabardi, S. Kumari, D. J. Irvine, *ACS Nano* **2017**, *11*, 3089.
[57] J. Thiery, D. Keefe, S. Boulant, E. Boucrot, M. Walch, D. Martinvalet, I. S. Goping, R. C. Bleackley, T. Kirchhausen, J. Lieberman, *Nat. Immunol.* **2011**, *12*, 770.